J. Solid Mech. 2026; 18(01): 59-72

Journal of Solid Mechanics

https://doi.org/10.57647/jsm.2026.1801.04

Research Article

ANN Simulation and Thermo-Flow Optimization of a Non-Polar Hybrid CuO Nanofluid

Mohammad Ali Fazilati[1,2*], Ali Mokhtarian[1,2], Mojtaba Rahimi[1,3*], Mohammad Hashemian[1,2]

[1]*Department of Mechanical Engineering, Kho.C., Islamic Azad University, Khomeinishahr, Iran*
[2]*Efficiency and Smartization of Energy Systems Research Center, Kho.C., Islamic Azad University, Khomeinishahr, Iran*
[3]*Stone Research Center, Kho.C., Islamic Azad University, Khomeinishahr, Iran*

***Corresponding author:** mrahimi@iau.ac.ir, ma.fazilati@iau.ac.ir

Article History:

Received:
01 October 2025

Revised:
20 February 2026

Accepted:
25 February 2026

Published in Issue:
31 March 2026

Abstract

Efficient thermal management is a cornerstone of modern industrial productivity, particularly in high-heat-flux applications such as chemical reactors and electronic cooling. Nanofluids (NFs) offer a transformative solution by enhancing the thermo-physical properties of conventional coolants; however, identifying optimal property configurations is vital for industrial feasibility. This research focuses on the modeling and optimization of a non-polar hybrid CuO / 1-4 dioxane + Diethyl amine (DEA) nanofluid with binary base fluids a system of significant interest for specialized organic-based heat transfer processes. The study utilizes experimental data to model dynamic viscosity (DV) and thermal conductivity (TC) across temperatures of 25°C to 45°C and solid volume fractions (SVF) of 0.01% to 0.06%. Two separate two-layer feedforward artificial neural networks (ANNs) were designed for prediction. The networks demonstrated exceptional reliability, with average relative errors of 0.3387% for DV and 0.3230% for TC. To provide a practical design tool for industrial engineers, a multi-objective optimization problem was solved using the MOPSO method to simultaneously maximize TC and minimize DV. The resulting Pareto optimal points represent a crucial decision-making framework, allowing for the selection of nanofluid concentrations that balance enhanced heat transfer with reduced pumping power costs. This work offers a robust simulation and optimization pathway for implementing non-polar nanofluids in high-efficiency industrial thermal systems.

Keywords: Nanofluid; Dynamic viscosity; Thermal conductivity; Artificial Neural Network; Multi-Objective Optimization

Cite this article: Fazilati, M. A., Mokhtarian, A., Rahimi, M., Hashemian, M., (2026) ANN Simulation and Thermo-Flow Optimization of a Non-Polar Hybrid CuO Nanofluid, *Journal of Solid Mechanics,* 18(01): 59-72, https://doi.org/10.57647/jsm.2026.1801.04

1. Introduction

The technology advancements give rise to an increasing demand for high heat transfer rates through small heat transfer surface areas. In heat exchanger systems, the need for concentrated heat transfer obliges the replacement of conventional heat transfer fluids (*HTF*s) with more efficient ones. A large number of studies are focusing on enhancing the thermal properties of *HTF* for the provision of efficient heat transfer [1]. Nanofluids (*NF*s), as the homogenous suspension of nanoparticles (*NP*s) of 1 to 100 nm in diameter, have emerged as an efficient replacement of conventional *HTF*s [2]. By their astonishing thermal properties, *NF*s have emerged as a promising alternative in heat transfer applications [3]. The most commonly used types of nanomaterials are metals [4], carbon-based materials (including single and multi-walled carbon nanotubes (*CNT*) [5], graphene [6]), and metal oxides [7]. The geometries of *NP*s employed could be spherical [8], cylindrical [9], rod form [10], wire form

[11], tubular [12], platelets [6], and plate [13]. By their higher chemical stability, lower density, and ease of preparation [14], metal oxides have been studied more than other materials. The base fluid includes water [15], ethylene glycol (*EG*) [16], mineral oil [17], molten salts [18], ionic liquids [19], propanol [20], dimethylformamide (*DMF*) [21], silicone-based liquids [22], and hydrochloro-fluoro-carbon (*HCFC*) [23]. Despite their desirable characteristics, the *NF*s application has some limitations, which are mainly due to increased dynamic viscosity (*DV*) caused by the presence of solid particles [24]. The elevated *DV* is undesirable for the thermal management goal since it increases the pressure losses. Generally, some factors affect the *NF*s properties such as base fluid properties [25], *NP* concentration, or in other term, solid volume fraction (*SVF*) [26], temperature [27], and *NP* shape [28]. Compared to other properties, the presence of *NP*s extremely affects the values of *DV* and *TC* of the fluid; hence, most studies on *NF* properties investigated these two properties [29]. General impact of temperature rise is respectively the increase and decrease of *TC* and *DV* and that for concentration is increasing of both values of *TC* and *DV* [30]. Most investigations in the field of *NF* are focused on single *NF*s which are the suspension of one *NP* type in a base fluid, and conventionally are referred to *NF*s. For the purpose of higher heat transfer enhancement, hybrid *NF*s are introduced which are composed of more-than-one *NP* type [31]. A large number of studies have been reported the measurement results of *DV* and *TC* of hybrid *NF*s. Taherialekouhi et al. [32], investigaated the *TC* of graphene oxide-Al_2O_3/water *NF* in volume concentration of 0.1% to 1% and temperature range of 25–50°C. They reported the highest improvement of *TC* as 33.9% for *SVF* of 1% and temperature of 50°C. The *TC* and *DV* of diamond-silver/ethylene glycol (*EG*) hybrid *NF* at temperature and concentration ranges of 10–60°C and 0–0.1% measured by Oliveira et al. [33]. They found the maximum *DV* and *TC* improvement percent as 21.21% and 6.92% and also declared the conditions of their occurrence. As the *HTF* for engine cooling, Yaw et al. [6] investigated the application of graphene nano-platelets-cellulose nanocrystals/40:60 solution of water and *EG* as the hybrid *NF*. They found 52% increment of convective heat transfer coefficient and heat exchanger size decrement as the result of implementing this *NF*. Venkatesh et al. [34] investigated three different hybrid *NF*s of water based Al_2O_3-SiO_2, SiO_2-*CuO*, and Al_2O_3-*CuO* in a solar desalination system equipped with flat plate collector. They reported that between the studied *NF*s, Al_2O_3-*CuO*/water has the most improving effect on sweet water production rate which was 41.7%. Experimental measurement of *TC* and *DV* is a tedious and time-consuming task. As a replacement, various models have been developed for predicting the *NF* properties. The factors that affect the quality and precision of modeling methods consist of the algorithm type, the input variables, and the data points. Among the methods in the field, the machine learning (*ML*) approach is the most famous and widely used [35]. This method has the subcategories of the artificial neural network (*ANN*), the multi-layer perceptron (*MLP*) *ANN*, the adaptive neuro-fuzzy inference system (*ANFIS*), the least square support vector machine (*LSSVM*), and the radial basis function (*RBF*). By its high accuracy and good prediction ability, the *ANN* method is mostly used for the purpose of *NF* properties prediction. In studies concerning *NF* properties estimation, one major subject is achieving the optimum condition; and for *NF* properties, the optimum state is that of the lowest and highest *DV* and *TC*, respectively. For assessing the optimal conditions, different optimization procedures could be employed in conjunction with *ANN* modeling. By the nonlinear nature of *NF* properties optimization problems, the conventional methods, such as trial-and-error and gradient-based algorithms, give suboptimal solutions; furthermore, they often impose costly computations and have limitations for handling multi-objective problems. Multi-objective particle swarm optimization (*MOPSO*) is an algorithm that is inspired by the social behavior of swarms and is used to find optimal solutions (Pareto front) in multiple conflicting objective problems [36]. *ANN* combined with *MOPSO* decreases the computational costs by approximating the complex relationships and problem constraints [37]. Petrudi and Rahmani [38] elaborated the *TC* and *DV* of an engine oil *NF* using the experimental and *ANN* modeling approaches. They aimed to find the *SVF* and temperature conditions for the achievement of maximum *TC* and minimum *DV*. In the non-dominated sorting genetic algorithm II (*NSGA* II) optimization algorithm, the R^2 value was determined as 0.9989; also, they reported the optimal conditions of *TC* and *DV* at a temperature of 333°C. Alsaady [39] employed response surface methodology (*RSM*) to assess the thermo-physical properties of diamond-nickel/*EG* *NF*. The input parameters were the *SVF* of *NP* and temperature, and the *MOPSO* was used as the optimization algorithm. They found the optimum *TC* and *DV* as 0.282 W/m.°C and 5.867 mPa·s, respectively, which were for a temperature and concentration of 60°C of 2.998 wt.%. Esfe et al. [40] studied the rheological behavior of *EG*-based *NF* of *MWCN-CuO* at different *SVF*s and temperatures. They declared different Newtonian/non-Newtonian behavior of the studied *NF* as a function of *SVF*. They also presented an empirical correlation for *DV,* which was found to be in good agreement with experimental data. Rostamzadeh-

10.57647/jsm.2026.1801.04

Renani et al. [36] utilized optimization algorithms of *NSGA* II, *MOPSO*, and the multi-objective grey wolf optimizer (*MOGWO*), along with the group method of data handling (*GMDH*) *ANN*s for the achievement of the optimum rheological behavior of *NF*. They used *SVF*, temperature, and shear rate as the network inputs and showed that the *GMDH ANN* with *MOGWO* coupling gives the best predictive performance, while the genetic algorithm (*GA*) yields the most optimal results. Hai et al. [41] conducted an optimization algorithm on graphene oxide/ iron oxide/ titanium dioxide hybrid *NF* by different *ML* techniques of multi-objective optimization, and multi-criteria decision-making. They also used *MOPSO* to find optimal *TC* and *DV* and their conditions. In addition to the application of more than one type of *NP* in hybrid *NF*s, sometimes a mixture of more than one type of base fluid is employed. Akhgar et al. [42] employed *ANN*s for *TC* prediction of *MWCNT*-TiO2/water-*EG* nanofluid. The base fluid was a 50:50 mixture of water/*EG,* and the diverse *ANN* architectures and training algorithms were also implemented. Their results showed close agreement with empirical data and also had better accuracy than conventional correlation equations. Esfe et al. [43] presented the multi-objective optimization of *TC* and *DV* of TiO_2/Bio-Glycol-water as a binary-fluid-based nanofluid. They employed the *NSGA-II* algorithm coupled with *RSM* and *ANN* and illustrated good prediction accuracy with regression coefficients of nearly 1. The optimization process revealed the optimum values of *TC* and *DV* at maximum temperature and *SVF*. Ru et al. [44] employed an *ML* model to predict the rheological behavior of *MWCNT*-Al_2O_3/water-*EG* nanofluid. A multilayer perceptron neural network (*MLPNN*) was used for *DV* prediction. The training parameters optimization was performed using algorithms of *GA*, *PSO*, and Marine Predators Algorithm (*MPA*). The evaluation indices demonstrated high prediction accuracy of the model and declared the *SVF* as the most prominent factor affecting *DV*. The present study aims to estimate and optimize the thermal-flow behavior of the *NF* made by dispersing *CuO* nanoparticles in a binary fluid of 1-4 Dioxane + diethyl amine (*DEA*) as a nonpolar hybrid *NF*. Despite the extensive literature on the thermal properties of nanofluids, the majority of existing research has focused on polar base fluids such as water, ethylene glycol, and oil. However, non-polar systems involving binary base fluids like 1-4 dioxane and Diethyl amine (DEA) remain significantly under-explored, despite their critical importance in specialized organic chemical processing and high-precision electronic cooling. Furthermore, while ANNs have been applied to predict nanofluid behavior, their integration with multi-objective optimization (MOPSO) to specifically resolve the conflict between thermal conductivity enhancement and viscosity-driven pumping power in this unique non-polar hybrid CuO system represents a distinct gap in the current state-of-the-art. This study addresses this gap by providing high-precision predictive modeling and a Pareto-based optimization framework specifically tailored for this non-standard chemical environment. This work attempts to fill this gap via modeling and optimization of rheological and thermal parameters, i.e., *DV* and *TC*, using two input factors: the temperature and the *VF*. In this way, these two properties are firstly modeled using the trained two-layer feedforward *ANN*s. For design, training, and evaluation of the model, the experimental data of Rohini [45] have been employed. At the next step, the *MOPSO* optimization process is used to achieve a set of optimal points. Figure 1 depicts the modeling and optimization stages taken in the present study.

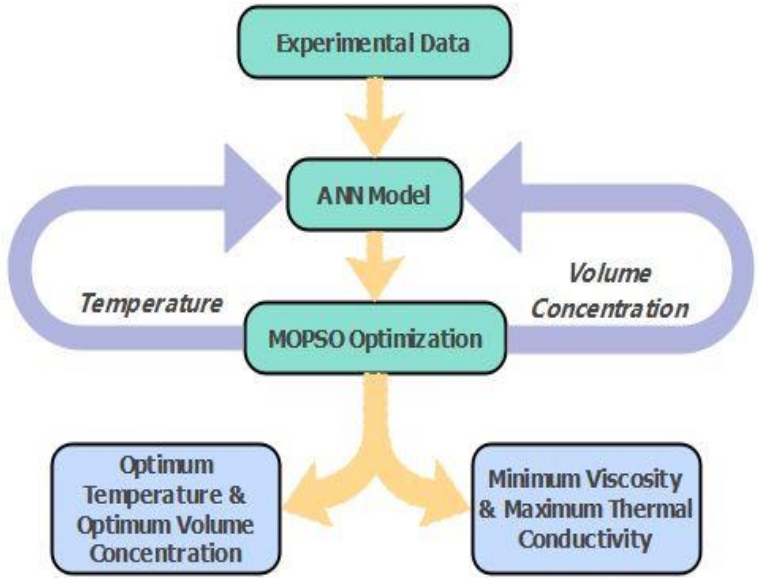

Figure 1. The block diagram of the ANN modeling and optimization process taken in this study

10.57647/jsm.2026.1801.04

2. Methodology

The *ANN* type chosen for this work is feedforward. In this method, information flow between the layers is unidirectional, and the input data flow is from input layer nodes toward the hidden layer nodes (if any) and then to output layer nodes without cycles or loops. In the modern feedforward *ANN* method, the training process takes place using the backpropagation method [46]. For developing an *ANN* to predict the *TC* and *DV* of *CuO* / 1-4 dioxane + *DEA*, two separate two-layer feedforward *ANN*s have been designed, each of which has three neurons in the hidden layer. These *ANN*s are designed, configured, and trained using *MATLAB* and are shown schematically in Figure 2. In fact, the *ANN* is designed for finding a relationship between input parameters (the temperature and *SVF)* and output ones (the *TC* and *DV)*. The *DV* and *TC* of the investigated *NF* have been measured previously at different temperatures and *SVF* [45]. The mathematical model of a neuron consists of the weights (w_{ij}), bias (b_i), and activation function (f). The data processing in neurons is according to Eq. (1).

$$Y_{p,i} = f\left(\sum_{j=1}^{n} w_{ij}x_j + b_i\right) \tag{1}$$

In this study, experimental datasets were used as the inputs for *TD* and *DV* networks, among which 60% used for training the *ANN*, 20% for validation, and the remaining 20% for testing. For the network training, the Levenberg-Marquardt optimization algorithm was utilized through the backpropagation error method. The algorithm specifically upgrades the weights and bias states; moreover, the network performance evaluation index and the mean squared error (*MSE*) are employed, whose definition is given by Eq. (2).

$$MSE = \frac{1}{n}\sum_{i=1}^{m}\left(Y_{e,i} - Y_{p,i}\right)^2 \tag{2}$$

m is the number of experimental data points and $Y_{e,i}$ and $Y_{p,i}$ are the ith input experimental and output data, respectively. During the training of *the ANN* and for adjusting its parameters, the Levenberg-Marquardt algorithm was implemented.

The application of this algorithm is for managing the loss functions (Eq. (3)) expressed as a sum of squared errors.

$$f = \sum_{i=1}^{k} {e_i}^2 \tag{3}$$

k is the number of training data. The Jacobian matrix of the loss function is defined as a matrix including the error derivatives with respect to weights:

$$\mathrm{J}_{i,j} = \frac{\partial e_i}{\partial w_j} \qquad i = 1, \dots, n \ , \ \ j = 1, \dots, p. \tag{4}$$

p is the number of network parameters. The loss function gradient vector could be written as:

$$\nabla f = 2\mathbf{J}^T \cdot \boldsymbol{e} \tag{5}$$

e is the error vector, and the Hessian matrix (**H**) can be estimated using the following equation:

$$\mathrm{H} \approx 2\mathrm{J}^T \cdot \mathrm{J} + \lambda \mathrm{I} \tag{6}$$

λ is a damping factor that is to make the Hessian matrix positive, and **I** is the identity matrix. In the Levenberg-Marquardt, the process of updating the network parameters could be expressed as given by Eq. (7);

$$\mathbf{w}^{(i+1)} = \mathbf{w}^{(i)} - \left(\mathbf{J}^{(i)T} \cdot \mathbf{J}^{(i)} + \lambda^{(i)}\mathbf{I}\right)^{-1} \cdot \left(2\mathbf{J}^{(i)T} \cdot \mathbf{e}^{(i)}\right) \tag{7}$$

To improve the *ANN* performance, and before the data processing, all experimental input and output variables were normalized to values between zero and one. The transfer functions employed in the hidden and output layers are Tangent Sigmoid and Linear, respectively. Moreover, the training stoppage criterion is set at the occurrence of validation performance failures to a total of 10.

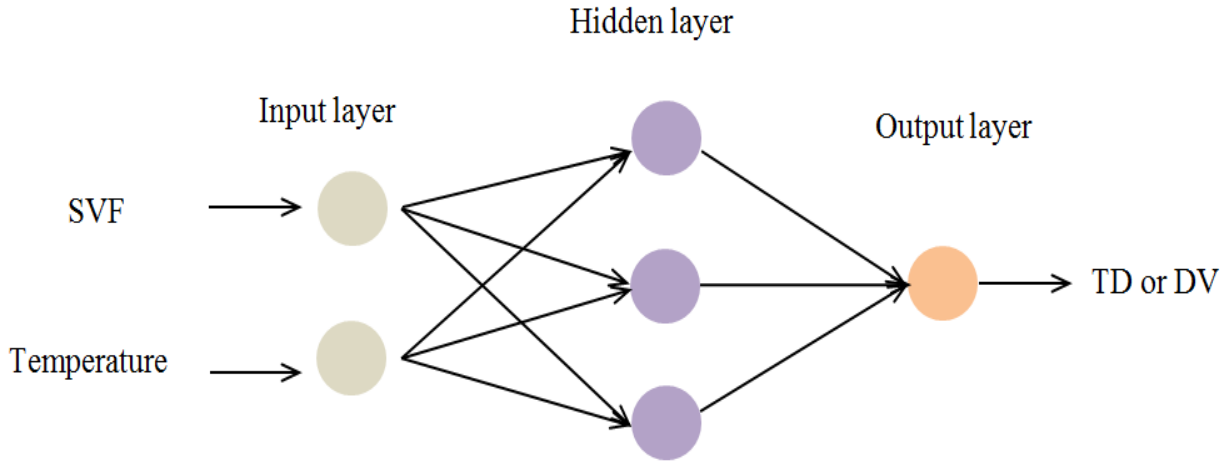

Figure 2. Architecture of a two-layer back-propagation neural network designed for the prediction of DV and TC

10.57647/jsm.2026.1801.04

3. Performance evaluation criteria

During the training process, the factor that shows the accuracy of the *ANN* is the *MSE* index. The variation of *MSE* during the training stage for the two *DV* and *TC* networks is depicted in Figure 3(a) and (b), respectively. For all sets of training, validation, and testing data of *DV* and *TC*-based networks, a decreasing trend for the *MSE* variation could be observed. In Figure 3(a) and (b), the best performance index is shown with a circle. The best *MSE* values for *DV* and *TC* networks are 8.0102×10^{-5} and 4.2292×10^{-4} at epoch 33 and 18, respectively. Moreover, the lowest values of *MSE* are between 4.4734×10^{-4} and 2.6738×10^{-4} for the *DV* and *TC* networks, respectively.

The other *ANN* evaluation index is the regression and correlation coefficients (*R*) between actual data and predicted values, whose variations for *DV* and *TC* are depicted in Figure 4 and Figure 5, respectively. These figures illustrate the *ANN* predicted values against the corresponding experimental ones for each of the training, validation, and test data sets. A well-trained *ANN* has the lowest *MSE* value, which shows almost the equality of predicted output to actual ones for all data points. Therefore, for a perfect network, having an *R* value and the regression line slope of one, the intercept (bias) of the regression line is zero. Considering the numerals shown in Figure 4 and Figure 5, the *ANN* output results for all data sets show good accuracy in predicting target values. The values of *R* for the *DV*-output *ANN* (Figure 4) are as follows: Training data: 0.99476, Validation data: 0.99713, Test data: 0.99552, All data: 0.99843. The corresponding *R* values for the *TC*-output *ANN* (Figure 5) are as follows: Training data: 0.99814, Validation data: 0.9985, Test data: 0.9982, All data: 0.99795. As seen, all values of *R* are nearly 1, showing the good performance of the designed *ANN* for *DV* and *TC* prediction of *NF*s at different temperatures and solid volume fractions (*SVF*s). Fitting plots and relative error percent of the *ANN* test data corresponding to each of the *DV* and *TC* network outputs are illustrated in Figure 6. The observed good agreement between the actual experimental and the predicted *ANN* output values demonstrates the high precision and performance of the *ANN* for *TC* and *DV* prediction of the investigated *NF*.

For the test data, the maximum value of relative error for the *DV* and *TC* prediction networks was determined as 0.5078% and 0.6871%, respectively; also, the corresponding mean values for relative error were 0.3387% and 0.3230%, respectively. These very small figures show the great ability of the trained *ANN* for predicting *DV* and *TC* of the concerned *NF* at different temperatures and concentrations.

The marked points shown in Figure 7 indicate the absolute difference between the *ANN* outputs and the actual values of *DV* and *TC,* which are plotted against the *NF* temperature and volume concentration. The minimum, maximum, and average absolute value of errors of *DV* estimation were determined as 4.8008×10^{-8} mPa.s, 0.0209 mPas, and 0.0064 mPa.s, respectively; also, the corresponding values for *TC* estimation were obtained as 8.5181×10^{-6} W/m.K, 0.0016 W/m.K, and 5.3565×10^{-4} W/m.K, respectively. The negligible estimation errors of *ANN* in the prediction of *DV* and *TC* again show its high modeling accuracy.

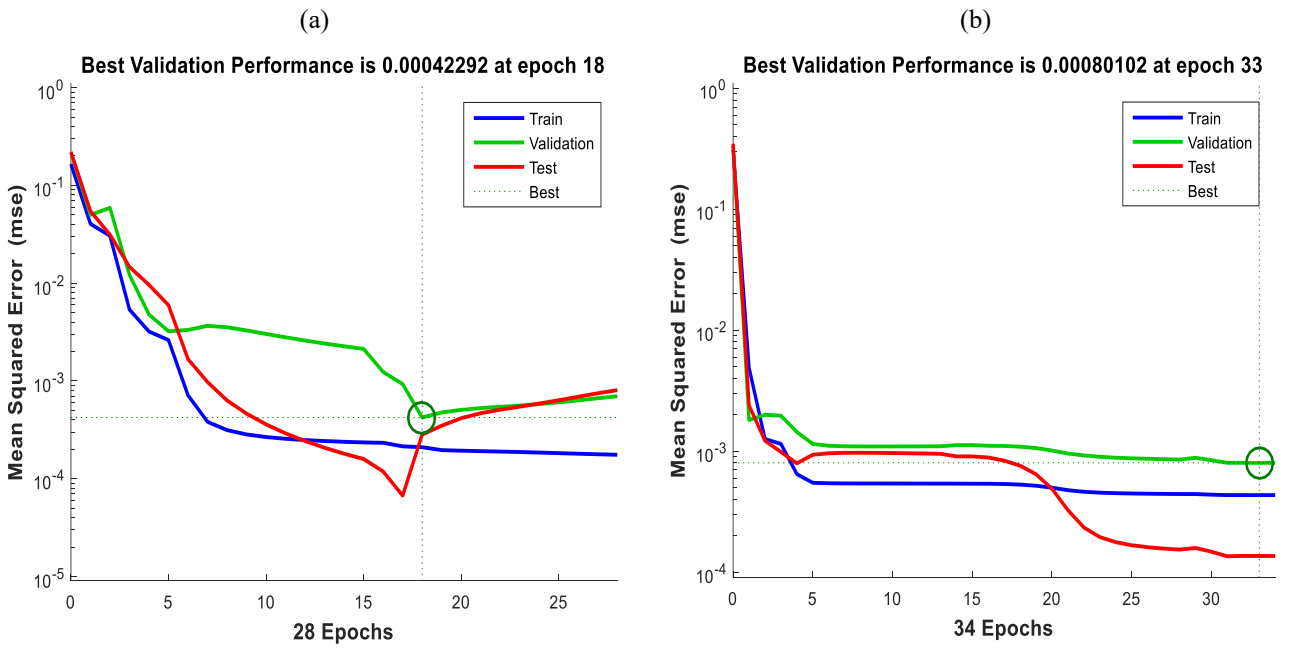

Figure 3. The variations of the MSE index corresponding to data sets of training, validation, and test data during the optimization stages for estimating a) DV and b) TC values

10.57647/jsm.2026.1801.04

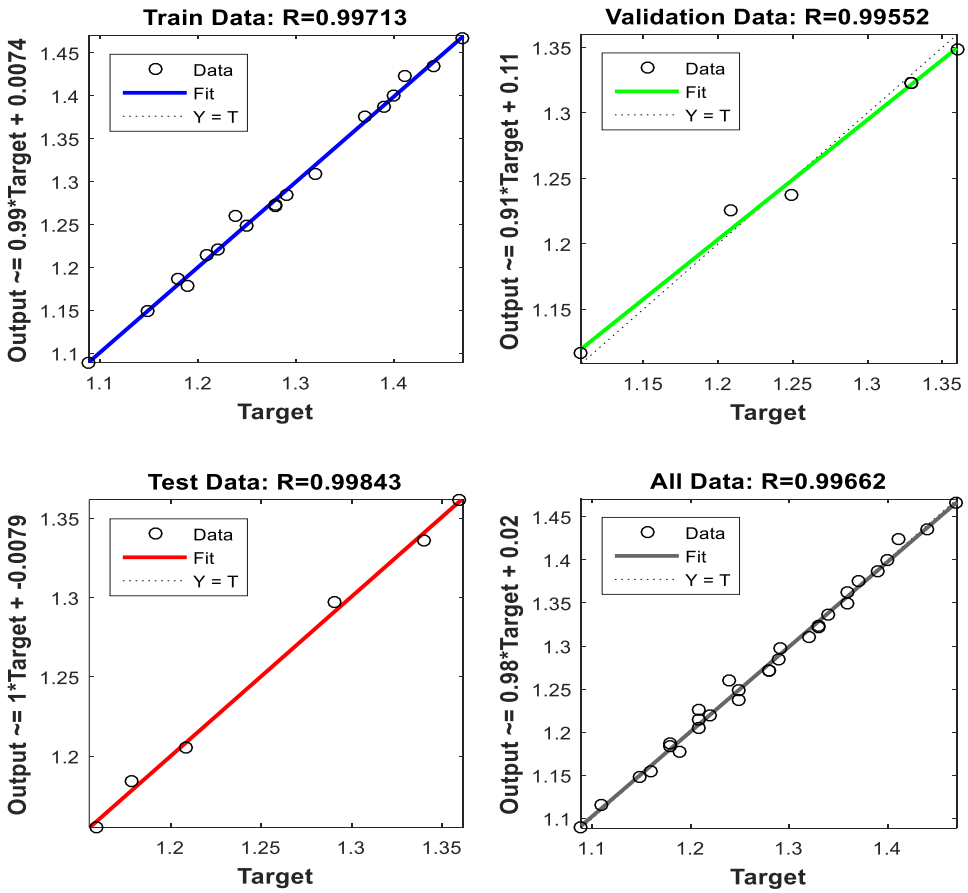

Figure 4. The *ANN* Regression plot corresponding to *DV* output for each set of training, validation, and test data

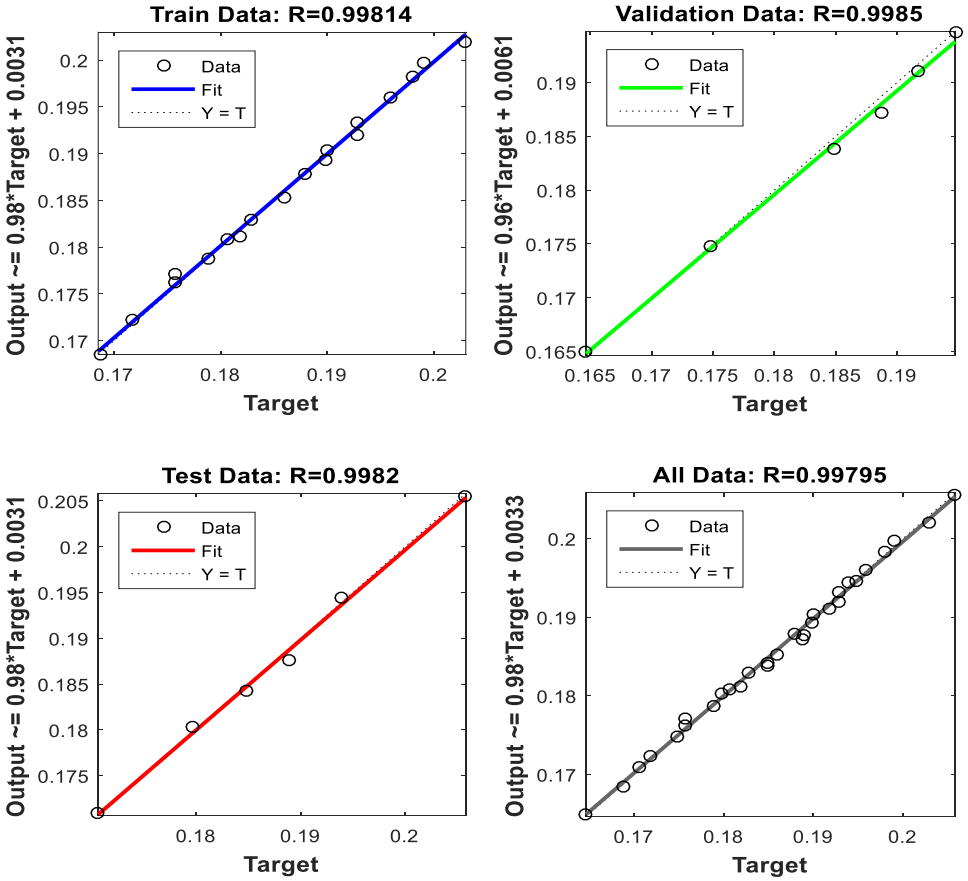

Figure 5. Regression plot of the *ANN* corresponding to the *TC* output for each set of training, validation, and test data

10.57647/jsm.2026.1801.04

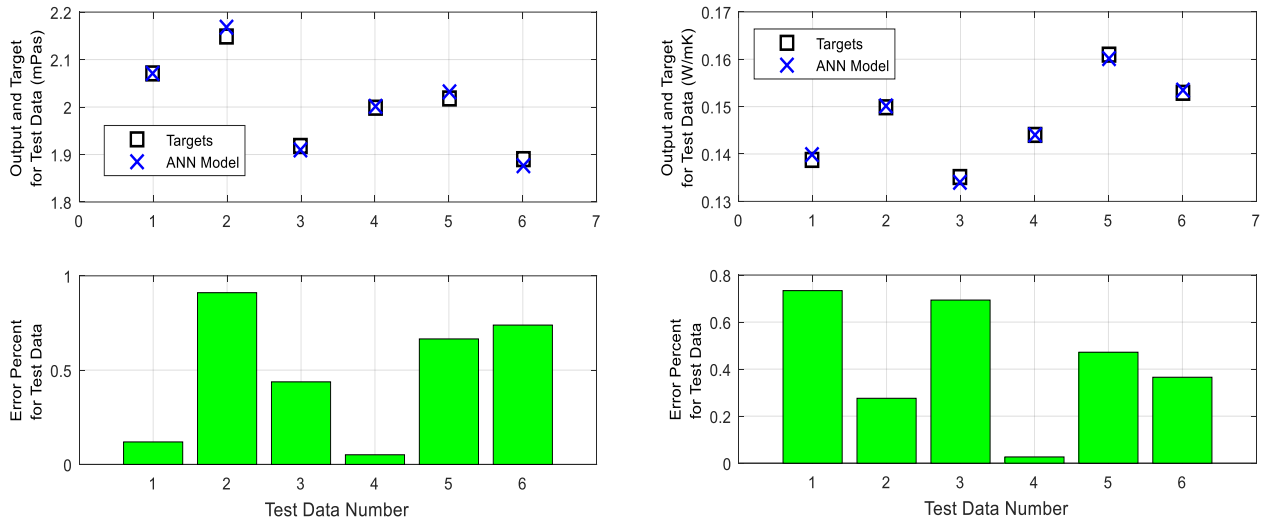

Figure 6. Fitting plots and relative error for top) DV and bottom) TC compared to the corresponding ANN outputs, for the test datasets

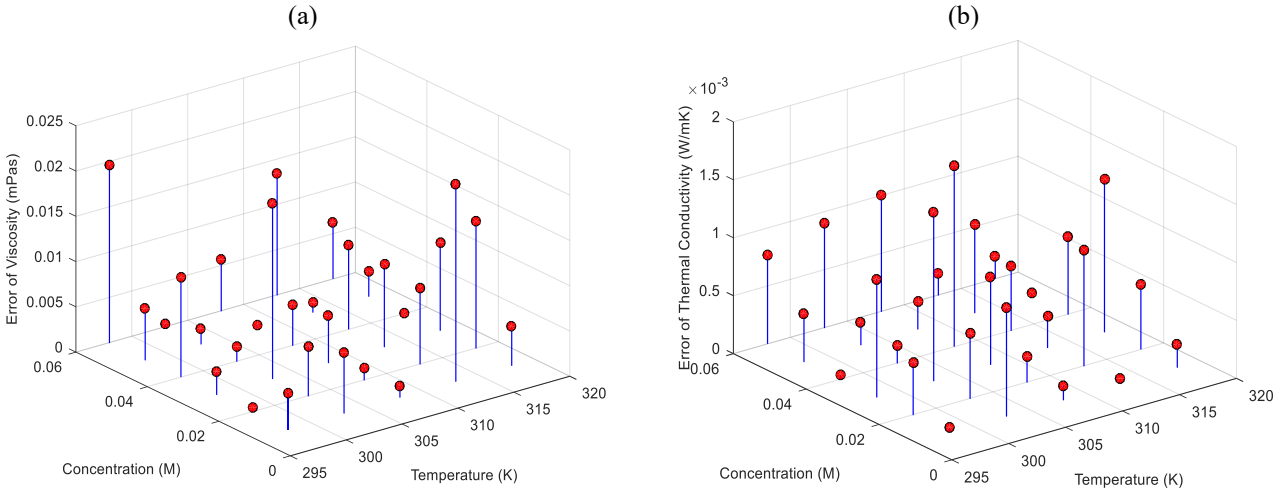

Figure 7. The variations of absolute error values of estimation a) *DV* and b) *TC* vs. the temperature and *SVF* for all data

4. The MOPSO optimization

In the *NF* application, the highest *TC* and the lowest *DV* are favorable [47]. Generally, the effect of temperature and *SVF* rise on the values of *TC* and *DV* is in reverse [48], and hence, finding the optimum situation is a major goal. In this section, a multi-objective optimization problem is presented and resolved to find the lowest *DV* and the highest *TC* of the studied *NF* using the Multi-Objective Particle Swarm Optimization (*MOPSO*) metaheuristic method. *MOPSO* is a direct method for solving multi-objective optimization problems that is faster than conventional methods. It can get a set of answers from which, and based on prioritizing the desired objective functions, the user can choose the best answer. Coello et al. [49] first proposed the *MOPSO* algorithm. This approach is the extension of the standard *PSO* algorithm, which handles multi-objective optimization problems by incorporating a Pareto Envelope and grid-making technique, like the Pareto Envelope-based Selection Algorithm. In *MOPSO*, particles exchange information and move towards both the best particles and their own personal best locations, showing the behavior of *PSO*. However, *MOPSO* differs in the way that it uses multiple criteria for specifying the "best" positions. Particularly, all non-dominated particles in the swarm are collected into a Repository, and each particle selects its global best target among the repository members.

A probabilistic rule based on the chosen domination is employed to determine each particle's best position [50]. The general flowchart of the *MOPSO* algorithm is illustrated in Figure 8. In the present work, the conflicting objective functions are the *DV* and *TC*, and the optimization variables include the *NF* temperature and *SVF*. The adjustment parameters along with their numerical values of the optimization algorithm are listed in Table 1. The code employed for implementing the algorithm was written in MATLAB software.

10.57647/jsm.2026.1801.04

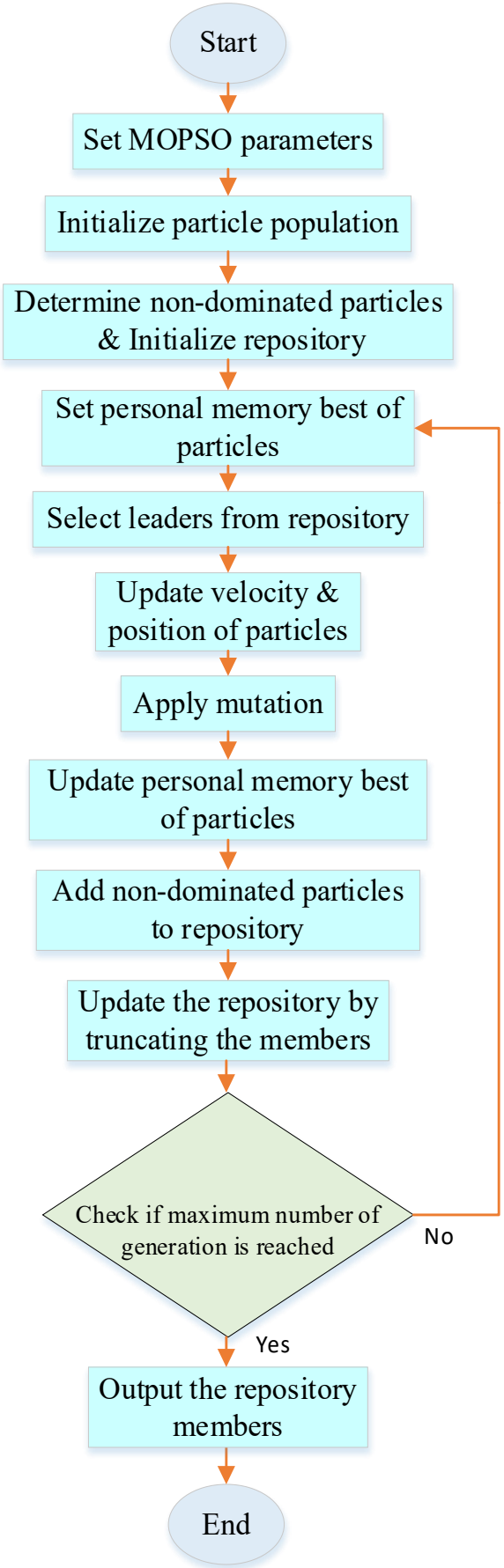

Figure 8. General flowchart diagram of the MOPSO algorithm

Table 1. The tuning parameter values used for the *MOPSO* algorithm

Parameter	Value
Maximum Number of Iterations	1000
Population Size	100
Repository Size	40
Inertia Weight	0.5
Inertia Weight Damping Rate	0.99
Personal Learning Coefficient	1
Global Learning Coefficient	2
Number of Grids per Dimension	5
Inflation Rate	0.1
Leader Selection Pressure	0.5
Deletion Selection Pressure	0.5
Mutation Rate	0.1

In Figure 9, the relationship between the objective function (DV and TC) at the Pareto optimal points is shown. Moreover, the numerical values of the objective functions corresponding to the Pareto optimal points with the corresponding input variables (NF temperature and SVF) are presented in Table 2. As seen, the optimal SVF values for the Pareto points are in the range of 0.0180 to 0.0351 percent, while the optimal temperature is nearly 45°C for all these points, which is the upper limit of the investigated temperature range. Besides, the variation range of optimum DV is very small and is between 1.8124 and 1.9963 mPa.s, and that for the optimum TC is between 1.1499 and 1.2052 W/m.K. Afterwards, it is the user's decision in prioritizing the objective functions (DV or TC), which determines the optimal situation between these points. It could also be seen that for the Pareto optimal points, increasing the TC resulted in a larger increase of DV, and decreasing TC is associated with a greater decrease of DV; this behavior is always expected for the Pareto points, considering the definition of dominance and that no Pareto point dominates another.

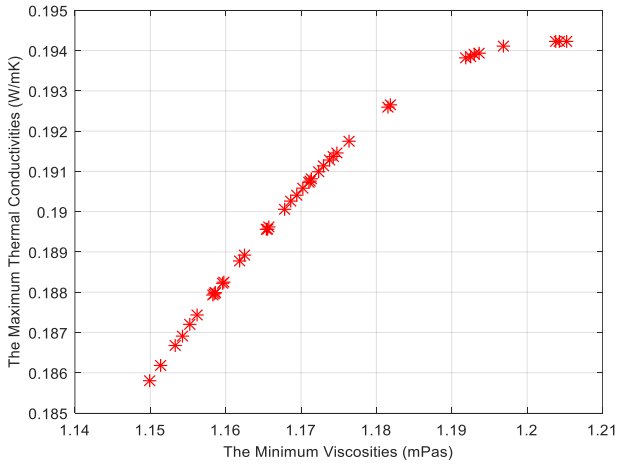

Figure 9. Pareto front of points resulting from the optimization of *DV* and *TC* using the *MOPSO* algorithm

10.57647/jsm.2026.1801.04

Table 2 Optimal temperature and SVF corresponding to the Pareto points obtained for the lowest DV and highest TC of the investigated NF

Point number	T_{opt} (˚C)	SVF_{opt} (%)	DV_{min} (mPa.s)	TC_{max} (W/m.K)
1	45.00	0.0255	1.1712	0.1908
2	45.00	0.0201	1.1553	0.1872
3	45.00	0.0347	1.2037	0.1942
4	45.00	0.0237	1.1657	0.1896
5	45.00	0.0264	1.1742	0.1914
6	45.00	0.0212	1.1585	0.1880
7	45.00	0.0224	1.1619	0.1888
8	45.00	0.0260	1.1730	0.1911
9	45.00	0.0351	1.2052	0.1942
10	45.00	0.0197	1.1542	0.1869
11	45.00	0.0348	1.2043	0.1942
12	45.00	0.0315	1.1918	0.1938
13	45.00	0.0252	1.1702	0.1906
14	45.00	0.0319	1.1931	0.1939
15	45.00	0.0266	1.1748	0.1915
16	45.00	0.0317	1.1925	0.1939
17	45.00	0.0254	1.1710	0.1907
18	45.00	0.0180	1.1499	0.1858
19	45.00	0.0211	1.1583	0.1879
20	45.00	0.0287	1.1818	0.1927
21	45.00	0.0204	1.1563	0.1874
22	45.00	0.0329	1.1968	0.1941
23	45.00	0.0216	1.1596	0.1882
24	45.00	0.0255	1.1714	0.1908
25	45.00	0.0263	1.1738	0.1913
26	45.00	0.0213	1.1586	0.1880
27	45.00	0.0321	1.1937	0.1939
28	45.00	0.0236	1.1654	0.1896
29	45.00	0.0244	1.1678	0.1901
30	45.00	0.0193	1.1533	0.1867
31	45.00	0.0236	1.1655	0.1896
32	45.00	0.0258	1.1723	0.1910
33	45.00	0.0249	1.1694	0.1904
34	45.00	0.0213	1.1586	0.1880
35	45.00	0.0271	1.1763	0.1917
36	45.00	0.0186	1.1513	0.1862
37	45.00	0.0216	1.1597	0.1883
38	45.00	0.0226	1.1625	0.1889
39	45.00	0.0286	1.1815	0.1926
40	45.00	0.0247	1.1687	0.1903

Figure 10(a) and (b) present the variations of the DV¬min and TCmax vs. the optimal temperature and SVF, corresponding to the obtained Pareto optimal points. It is seen that both the maximum TC and the minimum DV increased by increasing the SVF. Therefore, as can also be inferred from Table 2, the lowest DV¬min corresponds to the optimal point with the lowest SVF, and the highest TCmax corresponds to the optimal point with the highest SVF values.

Furthermore, the optimal temperature corresponding to all optimal points has been determined to be approximately 45°C.

10.57647/jsm.2026.1801.04

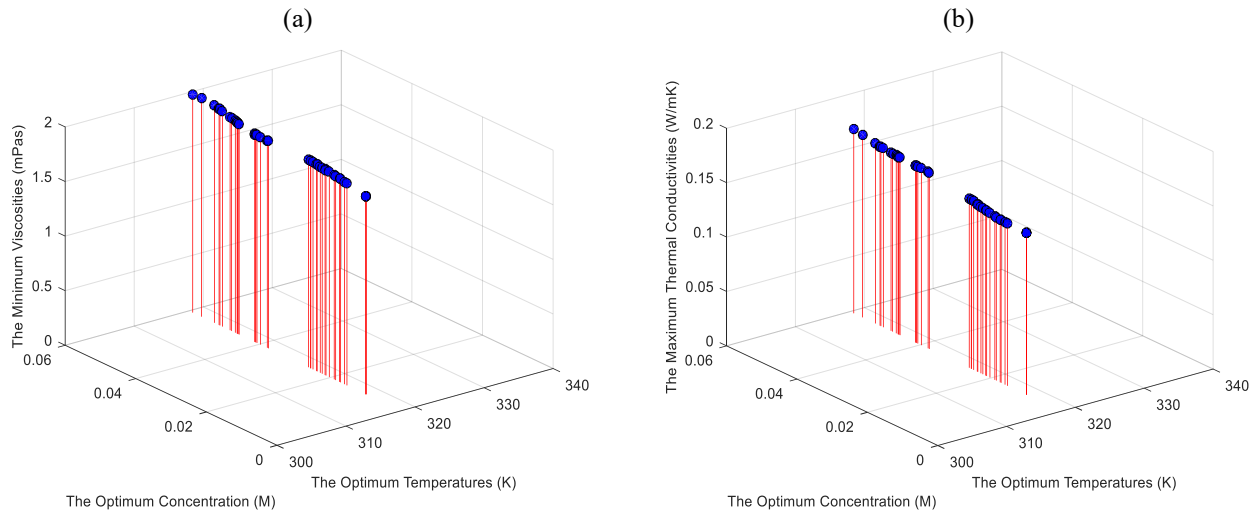

Figure. 10 Optimal values of the objective functions of (a) DV and (b) TC against the optimal input values for the corresponding Pareto points obtained from the MOPSO algorithm

5. Conclusions

This study developed a robust predictive and optimization framework for a non-polar CuO-based nanofluid (cyclohexane and 1-4 Dioxane) using ANNs and the MOPSO algorithm. The findings are summarized as follows:

1) The developed two-layer feedforward ANNs demonstrated exceptional reliability in predicting dynamic viscosity (DV) and thermal conductivity (TC). Both models achieved R-values exceeding 0.99 and very low Mean Squared Errors (MSE), with average relative errors on test data limited to 0.3387% for DV and 0.3230% for TC.

2) The MOPSO algorithm successfully identified a Pareto optimal front, resolving the trade-off between heat transfer enhancement and hydraulic resistance. Optimal solid volume fractions (SVF) were found to range between 0.0180% and 0.0351%.

3) Optimization results revealed that the upper limit of the investigated temperature range (45°C) is the most favorable for industrial application, as it simultaneously yields the maximum thermal conductivity (0.1942 W/m·K) and minimum dynamic viscosity (1.1492 mPa·s). The proposed ANN-MOPSO approach provides a reliable decision-making tool for industrial designers, allowing for the precise selection of nanofluid parameters to balance thermal efficiency with pumping power requirements.

Nomenclature

Al_2O_3	Aluminum oxide
ANFIS	Adaptive neuro-fuzzy inference system
ANN	Artificial neural network
b	bias
CuO	Copper oxide
DEA	diethyl amine
DMF	dimethylformamide
DV	Dynamic viscosity
EG	Ethylene glycol
GA	Genetic algorithm
HCFC	Hydro Chloro Fluoro Carbon
k	Thermal conductivity (W/m.K)
LSSVM	The least square support vector machine
m	Number of training data
MLP	Multi-layer perceptron
MPA	Marine predators algorithm
GMDH	Group method of data handling
MOGWO	Multi-objective grey wolf optimizer
MOPSO	Multi-objective particle swarm optimization
MWCNT	Multi-walled carbon nanotube
NF	Nanofluid
NN	Neural network
NP	Nanoparticle
NSGA-II	Non-dominated sorting genetic algorithm II
RSM	response surface methodology
SVF	Solid volume fraction (%)
TC	Thermal conductivity (W/m.K)
T	Temperature (K)
w	Weight (kg)

Authors Contribution

All the authors have participated sufficiently in the intellectual content, conception and design of this work or the analysis and interpretation of the data (when applicable), as well as the writing of the manuscript.

Availability of data and materials

The data that support the findings of this study are available from the corresponding author, upon reasonable request.

Conflict of interests

The author states that there is no conflict of interest.

10.57647/jsm.2026.1801.04

References

[1] Miansari, M., Jafari, S. S., Alizadeh, A. A., & Fazilati, M. A. (2023). Hydrothermal behavior of different hybrid nanofluids in a dimpled tube heat exchanger. Engineering Analysis with Boundary Elements, 157, 21-33. https://doi.org/10.1016/j.enganabound.2023.08.035

[2] Zeeshan, A., Shehzad, N., Ellahi, R., & Alamri, S. Z. (2018). Convective Poiseuille flow of Al2O3-EG nanofluid in a porous wavy channel with thermal radiation. Neural Computing and Applications, 30, 3371-3382. https://doi.org/10.1007/s00521-017-2924-9

[3] Irandoost Shahrestani, M., Maleki, A., Safdari Shadloo, M., & Tlili, I. (2020). Numerical investigation of forced convective heat transfer and performance evaluation criterion of Al2O3/water nanofluid flow inside an axisymmetric microchannel. Symmetry, 12(1), Article 120. https://doi.org/10.3390/sym12010120

[4] Xuan, Y., Li, Q., & Tie, P. (2013). The effect of surfactants on heat transfer feature of nanofluids. Experimental Thermal and Fluid Science, 46, 259-262. https://doi.org/10.1016/j.expthermflusci.2012.12.004

[5] Chereches, E. I., Bejan, D., & Minea, A. A. (2023). Experimental on viscosity and isobaric heat capacity of [C4mim][BF4] ionic liquid with MWCNT nanoparticles. Journal of Molecular Liquids, 391, Article 123214. https://doi.org/10.1016/j.molliq.2023.123214

[6] Yaw, C. T., Koh, S., Sandhya, M., Kadirgama, K., Tiong, S. K., Ramasamy, D., Sudhakar, K., Samykano, M., Benedict, F., & Tan, C. H. (2023). Heat transfer enhancement by hybrid nano additives graphene nanoplatelets/cellulose nanocrystal for the automobile cooling system (radiator). Nanomaterials, 13(5), Article 808. https://doi.org/10.3390/nano13050808

[7] López-Domínguez, P., Díez-Sierra, J., Schäfer, S., Schunk, S. A., Bäcker, M., De Buysser, K., Van Driessche, I., & Rijckaert, H. (2024). Size-controlled oxide perovskite nanocrystal synthesis: Design, optimization, and mechanism insights. Crystal Growth & Design, 24(6), 2362-2369. https://doi.org/10.1021/acs.cgd.3c01273

[8] Zhang, H., Qing, S., Xu, J., Zhang, X., & Zhang, A. (2022). Stability and thermal conductivity of TiO2/water nanofluids: A comparison of the effects of surfactants and surface modification. Colloids and Surfaces A: Physicochemical and Engineering Aspects, 641, Article 128492. https://doi.org/10.1016/j.colsurfa.2022.128492

[9] Yang, B., & Han, Z. (2006). Temperature-dependent thermal conductivity of nanorod-based nanofluids. Applied Physics Letters, 89(8), Article 083111. https://doi.org/10.1063/1.2338424

[10] Ahmadipour, M., Ardani, M. R., Pang, A. L., Wee, M. F. M. R., & Satgunam, M. (2024). Removal of antibiotic sulfamethoxazole in water using rapid growing ZnO nanorod. Ceramics International, 50(16), 27645-27653. https://doi.org/10.1016/j.ceramint.2024.04.405

[11] Murshed, S. S. (2025). Thermal properties and features of nanofluids. MDPI.

[12] Sang, L., Ai, W., Wu, Y., & Ma, C. (2020). Enhanced specific heat and thermal conductivity of ternary carbonate nanofluids with carbon nanotubes for solar power applications. International Journal of Energy Research, 44(1), 334-343. https://doi.org/10.1002/er.4923

[13] Carrillo-Berdugo, I., Midgley, S. D., Grau-Crespo, R., Zorrilla, D., & Navas, J. (2020). Understanding the specific heat enhancement in metal-containing nanofluids for thermal energy storage: Experimental and ab initio evidence for a strong interfacial layering effect. ACS Applied Energy Materials, 3(9), 9246-9256. https://doi.org/10.1021/acsaem.0c01556

[14] Mirahmad, A., Kumar, R. S., Doldán, B. P., Rios, C. P., & Díez-Sierra, J. (2025). Beyond thermal conductivity: A review of nanofluids for enhanced energy storage and heat transfer. Nanomaterials, 15(4), Article 302. https://doi.org/10.3390/nano15040302

[15] Selvan, P., Jebakani, D., Jeyasubramanian, K., & Jones Joseph Jebaraj, D. (2022). Enhancement of thermal conductivity of water based individual and hybrid SiO2/Ag nanofluids with the usage of calcium carbonate nano particles as stabilizing agent. Journal of Molecular Liquids, 345, Article 117846. https://doi.org/10.1016/j.molliq.2021.117846

[16] Ahsan, M., Qamar, A., Shaukat, R., Siddiqi, H.-u.-R., Anwar, Z., Farooq, M., Amjad, M., Imran, S., Ahmed, M., Mujtaba, M. A., Fayaz, H., & Souayeh, B. (2024). Thermal and hydraulic performance of ZnO/EG based nanofluids in mini tubes of different diameters: An experimental investigation. Heliyon, 10(5), Article e26493. https://doi.org/10.1016/j.heliyon.2024.e26493

[17] Gangadhar, K., Naga Chandrika, G., & Dinarvand, S. (2025). Investigation into silver-engine oil nanoliquid convinced by Riga surface: Deviations in three binary nanofluids. Modern Physics Letters B, 39(2), Article 2450385. https://doi.org/10.1142/s0217984924503858

[18] Li, Z., Cui, L., Li, B., & Du, X. (2021). Mechanism exploration of the enhancement of thermal energy storage in molten salt nanofluid. Physical Chemistry Chemical Physics, 23(23), 13181-13189. https://doi.org/10.1039/d1cp00125f

[19] Minea, A. A., & Chereches, E. I. (2024). Experimental studies on thermal conductivity and heat transfer of 1-Butyl-3-methylimidazolium tetrafluoroborate ionic liquid and its nanocolloids. International Communications in Heat and Mass Transfer, 154, Article 107406. https://doi.org/10.1016/j.icheatmasstransfer.2024.107406

[20] Strandberg, R., Ray, D., & Das, D. K. (2024). Experimental characterization of hydronic air coil performance with aluminum oxide nanofluids of three concentrations. Applied Nano, 5(2), 84-107. https://doi.org/10.3390/applnano5020008

[21] Rodríguez-Laguna, M. R., Castro-Alvarez, A., Sledzinska, M., Maire, J., Costanzo, F., Ensing, B., Pruneda, M., Ordejón, P., Sotomayor Torres, C. M., Gómez-Romero, P., & Chávez-Ángel, E. (2018). Mechanisms behind the enhancement of thermal properties of graphene nanofluids. Nanoscale, 10(32), 15402-15409. https://doi.org/10.1039/c8nr02762e

[22] De los Santos, D., Gallardo, J. J., Carrillo-Berdugo, I., Alcántara, R., Estellé, P., Gragera, S., Gragera, M., & Navas, J. (2024). Nanofluids based on Pd nanoparticles and a linear silicone-based fluid: Toward highly efficient heat transfer fluids for concentrated solar power. ACS Sustainable Chemistry & Engineering, 12(6), 2375-2385. https://doi.org/10.1021/acssuschemeng.3c07285

[23] Trisaksri, V., & Wongwises, S. (2009). Nucleate pool boiling heat transfer of TiO2–R141b nanofluids. International Journal of Heat and Mass Transfer, 52(5-6), 1582-1588. https://doi.org/10.1016/j.ijheatmasstransfer.2008.07.041

[24] Ramezanizadeh, M., Ahmadi, M. A., Ahmadi, M. H., & Alhuyi Nazari, M. (2019). Rigorous smart model for predicting dynamic viscosity of Al2O3/water nanofluid. Journal of Thermal Analysis and Calorimetry, 137, 307-316. https://doi.org/10.1007/s10973-018-7916-1

[25] Komeilibirjandi, A., Raffiee, A. H., Maleki, A., Alhuyi Nazari, M., & Safdari Shadloo, M. (2020). Thermal conductivity prediction of nanofluids containing CuO nanoparticles by using correlation and artificial neural network. Journal of Thermal Analysis and Calorimetry, 139, 2679-2689. https://doi.org/10.1007/s10973-019-08838-w

[26] Maheshwary, P., Handa, C., & Nemade, K. (2017). A comprehensive study of effect of concentration, particle size and particle shape on thermal conductivity of titania/water based nanofluid. Applied Thermal Engineering, 119, 79-88. https://doi.org/10.1016/j.applthermaleng.2017.03.054

[27] Shamaeil, M., Firouzi, M., & Fakhar, A. (2016). The effects of temperature and volume fraction on the thermal conductivity of functionalized DWCNTs/ethylene glycol nanofluid: An experimental study. Journal of Thermal Analysis and Calorimetry, 126, 1455-1462. https://doi.org/10.1007/s10973-016-5548-x

[28] Jeong, J., Li, C., Kwon, Y., Lee, J., Kim, S. H., & Yun, R. (2013). Particle shape effect on the viscosity and thermal conductivity of ZnO nanofluids. International Journal of Refrigeration, 36(8), 2233-2241. https://doi.org/10.1016/j.ijrefrig.2013.07.024

[29] Rashidi, M. M., Nazari, M. A., Mahariq, I., Assad, M. E. H., Ali, M. E., Almuzaiqer, R., Nuhait, A., & Murshid, N. (2021). Thermophysical properties of hybrid nanofluids and the proposed models: An updated comprehensive study. Nanomaterials, 11(11), Article 3084. https://doi.org/10.3390/nano11113084

[30] Ayoob, H. W., Omar, I., Ghanim, W. K., Fares, M. N., Fazilati, M. A., Salahshour, S., & Esmaeili, S.

(2025). The thermal-flow performance of water-Al2O3 nanofluid flow in an elliptical duct heat exchanger equipped with two rotating twisted tapes. Case Studies in Chemical and Environmental Engineering, 11, Article 101094. https://doi.org/10.1016/j.cscee.2025.101094

[31] Kshirsagar, D. P., & Venkatesh, M. (2021). A review on hybrid nanofluids for engineering applications. Materials Today: Proceedings, 44(Part 1), 744-755. https://doi.org/10.1016/j.matpr.2020.10.637

[32] Taherialekouhi, R., Rasouli, S., & Khosravi, A. (2019). An experimental study on stability and thermal conductivity of water-graphene oxide/aluminum oxide nanoparticles as a cooling hybrid nanofluid. International Journal of Heat and Mass Transfer, 145, Article 118751. https://doi.org/10.1016/j.ijheatmasstransfer.2019.118751

[33] de Oliveira, L. R., Ribeiro, S. R. F. L., Reis, M. H. M., Cardoso, V. L., & Bandarra Filho, E. P. (2019). Experimental study on the thermal conductivity and viscosity of ethylene glycol-based nanofluid containing diamond-silver hybrid material. Diamond and Related Materials, 96, 216-230. https://doi.org/10.1016/j.diamond.2019.05.004

[34] Venkatesh, R., Hossain, I., Mohanavel, V., Soudagar, M. E. M., Alharbi, S. A., & Al Obaid, S. (2024). Flat plate solar collector activated with alumina-silicon dioxide-copper oxide hybrid nanofluid: Thermal performance study. Applied Thermal Engineering, 257(Part B), Article 124496. https://doi.org/10.1016/j.applthermaleng.2024.124496

[35] Maleki, A., Haghighi, A., Irandoost Shahrestani, M., & Abdelmalek, Z. (2021). Applying different types of artificial neural network for modeling thermal conductivity of nanofluids containing silica particles. Journal of Thermal Analysis and Calorimetry, 144, 1613-1622. https://doi.org/10.1007/s10973-020-09541-x

[36] Rostamzadeh-Renani, R., Jasim, D. J., Baghoolizadeh, M., Rostamzadeh-Renani, M., Andani, H. T., Salahshour, S., & Baghaei, S. (2024). Multi-objective optimization of rheological behavior of nanofluids containing CuO nanoparticles by NSGA II, MOPSO, and MOGWO evolutionary algorithms and Group Method of Data Handling Artificial neural networks. Materials Today Communications, 38, Article 107709. https://doi.org/10.1016/j.mtcomm.2023.107709

[37] Esfe, M. H., Esfandeh, S., Amoozadkhalili, F., & Toghraie, D. (2023). Increasing the accuracy of estimating the dynamic viscosity of hybrid nano-lubricants containing MWCNT-MgO by optimizing using an artificial neural network. Arabian Journal of Chemistry, 16(1), Article 104405. https://doi.org/10.1016/j.arabjc.2022.104405

[38] Petrudi, A. M., & Rahmani, M. (2020). Validation and optimization of thermophysical properties for thermal conductivity and viscosity of nanofluid engine oil using neural network. Journal of Modeling and Simulation of Materials, 3(1), 53-60. https://doi.org/10.21467/jmsm.3.1.53-60

[39] Alsaady, M. (2021). Modeling and multi-objective optimization of thermophysical parameters of hybrid nanodiamond–Ni-based nanofluids via response surface methodology. Frontiers in Mechanical Engineering, 7, Article 675511. https://doi.org/10.3389/fmech.2021.675511

[40] Esfe, M. H., Motallebi, S. M., & Toghraie, D. (2022). A novel experimental and statistical study on ethylene glycol-based nanofluid enriched by MWCNT and CuO nanoparticles. Annals of Nuclear Energy, 177, Article 109283. https://doi.org/10.1016/j.anucene.2022.109283

[41] Hai, T., Basem, A., Alizadeh, A. A., Singh, P. K., Rajab, H., Maatki, C., Becheikh, N., Kolsi, L., Singh, N. S. S., & Maleki, H. (2025). Optimizing ternary hybrid nanofluids using neural networks, gene expression programming, and multi-objective particle swarm optimization: A computational intelligence strategy. Scientific Reports, 15, Article 1986. https://doi.org/10.1038/s41598-025-19598-z

[42] Akhgar, A., Toghraie, D., Sina, N., & Afrand, M. (2019). Developing dissimilar artificial neural networks (ANNs) to prediction the thermal conductivity of MWCNT-TiO2/ethylene glycol hybrid nanofluid. Powder Technology, 355, 602-610. https://doi.org/10.1016/j.powtec.2019.07.086

[43] Hemmat Esfe, M., Hatami, H., Kiannejad Amiri, M., Alidoust, S., Toghraie, D., & Esfandeh, S. (2023). Multi-objective optimization of viscosity and thermal conductivity of TiO2/BioGlycol-Water nanofluids with sorting non-dominated genetic algorithm II coupled with response surface methodology. Materials Today Communications, 36, Article 106718.

https://doi.org/10.1016/j.mtcomm.2023.106718

[44] Ru, Y., Ali, A. B., Qader, K. H., Abdulaali, H. K., Jhala, R., Ismailov, S., Salahshour, S., & Mokhtarian, A. (2025). Accurate prediction of the rheological behavior of MWCNT-Al2O3/water-ethylene glycol nanofluid with metaheuristic-optimized machine learning models. International Journal of Thermal Sciences, 211, Article 109691. https://doi.org/10.1016/j.ijthermalsci.2025.109691

[45] Rohini, B., Jeevaraj, A. K. S., Suvitha, A., Sangeetha, R., & Revathi, V. (2024). Optimization of thermal and rheological performance in non-polar binary fluids using hybrid CuO nanoparticles. Journal of Physics: Conference Series, 012010. https://doi.org/10.1088/1742-6596/2886/1/012010

[46] Schmidhuber, J. (2015). Deep learning in neural networks: An overview. Neural Networks, 61, 85-117. https://doi.org/10.1016/j.neunet.2014.09.003

[47] Abed, H., Ali Fazilati, M., Toghraie, D., Pirmoradian, M., & Mehmandoust, B. (2022). Molecular dynamics study of the thermal behavior of ammonia refrigerant in the presence of copper nanoparticles at different volume ratios and initial temperatures. Journal of Molecular Modeling, 28(6), Article 157. https://doi.org/10.1007/s00894-022-05156-1

[48] Hashempour, S., Toghraie, D., & Fazilati, M. A. (2023). Investigation of the thermal characteristics of water-based hybrid and mono nanofluids containing cerium oxide-CuO-MWCNT nanoparticles at various temperatures and volume fraction of nanoparticles and propose a new relationship. Journal of Materials Research and Technology, 26, 1276-1292. https://doi.org/10.1016/j.jmrt.2023.07.224

[49] Coello, C. A. C., Pulido, G. T., & Lechuga, M. S. (2004). Handling multiple objectives with particle swarm optimization. IEEE Transactions on Evolutionary Computation, 8(3), 256-279. https://doi.org/10.1109/tevc.2004.826067

[50] Coello, C. A. C., Lamont, G. B., & Van Veldhuizen, D. A. (2007). Evolutionary algorithms for solving multi-objective problems (2nd ed.). Springer. https://doi.org/10.1007/978-1-4757-5184-0